Erschienen in: ACS Applied Polymer Materials. ACS Publications. 2021, 3(10), S. 5243-5256
https://doi.org/10.1021/acsapm.1c01025

Unlayered−Layered Crystal Transition in Recyclable Long-Spaced Aliphatic Polyesters

Stephanie F. Marxsen, Manuel Häußler, Stefan Mecking, and Rufina G. Alamo*

ABSTRACT: We report the first known instance where the formation of layered crystals in long-spaced polyesters is bypassed on rapid quenching. Aliphatic polyesters spaced by 18−48 carbons in both the diol and diacid components of the repeating unit form orthorhombic, highly symmetric, layered crystals on relatively slow or isothermal crystallization. Though the unit cell is maintained on rapid quenching to 0 °C and lamellar crystals still form, the X-ray reflection of the ester layer disappears in PE-48,48 and weakens in the shorter-spaced polyesters. Since all crystal thicknesses are larger than the distance between the two consecutive esters, the esters must be inside the crystals in a random distribution. On heating, such unlayered crystals transform into the layered type at temperatures between 45 and 60 °C, which further melt at 98−115 °C with an increasing methylene spacer in the polyester. Rapidly quenched PE-48,48 develops only the unlayered structure, while shorter-spaced polyesters form mixed unlayered and layered crystals, indicating that a larger depth of quenching is required for the development of the unlayered form with decreasing CH_2 spacer length. We posit that on fast crystallization, metastable lamellar crystals form via staggering of chain segments and random chain folding, locking a structure where the ester groups are unlayered, while on slower crystallization, ester layering is facilitated by maximizing packing of the full length of CH_2 units via van der Waals interactions and intermolecular dipolar interactions of ester units. The discovery of unlayered, metastable structures of polyethylene-like materials developed under fast cooling from the melt is important for applications that mimic those which currently utilize commercial polyethylenes and that would benefit from sustainable monomer sources and material recyclability.

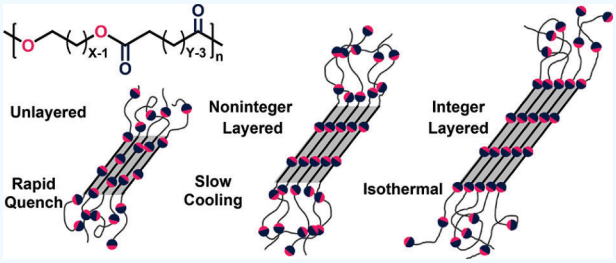

KEYWORDS: *aliphatic polyesters, long-spaced, fast quenching, crystallization, crystalline structure*

INTRODUCTION

In recent years, biosourced and biodegradable aliphatic polyesters have been identified as sustainable alternatives to a variety of commodity polymers synthesized from fossil fuels. Polyesters such as poly(lactic acid), poly(4-hydroxybutyrate), and poly(ε-caprolactone) have found uses in a diverse range of applications, from packaging and textiles to biomedical and tissue engineering.[1−4] Most aliphatic polyesters are semicrystalline, meaning comprehensive studies of their crystallization and melting processes, including crystallization kinetics, crystal structure, polymorphism, morphology, etc., are required for effective tuning of the desired physical properties and ultimate material performance.

The diversity of chemical structures possible in aliphatic polyesters makes for a complex range of crystallization behavior. Poly(hydroxyacid)s have the simplest repeating monomer unit of $-(C{=}O)-(CH_2)_X-O-$, while the structure of poly(alkylene dicarboxylate)s depends on the length of both the diol and diacid segments, i.e., $-O-(CH_2)_X-O-(C{=}O)-(CH_2)_{Y-2}-(C{=}O)-$. Recent advances in catalysis have enabled the synthesis of polyesters with increasingly long aliphatic segments; poly(alkylene dicarboxylate)s have been synthesized with up to $X = Y = 48$.[5]

While many short-spaced aliphatic polyesters have been studied, those with X and Y >∼13 have not been considered in as much detail, in part because of synthetic difficulties and in part because of the desire for biodegradability in some applications, which diminishes in aliphatic polyesters with longer CH_2 sequences due to increased crystallinity and hydrophobicity.[6−8] For instance, van der Meulen et al. studied the hydrolytic degradation of poly(pentadecalactone) (PE-14) and poly(hexadecalactone) (PE-15) in a phosphate-buffered saline (PBS) solution at physiological conditions (37 °C, pH = 7.4).[8] From the negligible mass loss and unchanged level of crystallinity, they concluded that the long aliphatic sequences prevented ester group hydrolysis even after a period of 2 years.

Furthermore, enzymatic degradation studies using *Pseudomonas cepacia* lipase (Lipase PS) in PBS also showed no detectable mass loss over 100 days. In contrast, the amorphous regions of polycaprolactone (PCL) undergo biodegradation more readily.[8]

Not only do long-spaced aliphatic polyesters display long-term stability, as shown by the above-mentioned biodegradation studies, but they also display unique chemical recyclability. We recently demonstrated that a small number of functional group "breakpoints" incorporated into a polyethylene backbone chain enable chemical recycling by solvolysis with a monomer recovery rate >96%.[9] This is drastic improvement over the chemical recyclability of linear polyethylene, which requires high temperatures (>600 °C) and produces substantially lower ethylene yields. Chemical recycling was accomplished in the long-spaced aliphatic polyester (LSAPE) PE-18,18 (as well as its analogue polycarbonate, PC-18) with quantitative monomer recovery at modest temperatures between 120 and 150 °C.[9]

The fact that PE-18,18 can be chemically recycled is especially significant since, with sufficient aliphatic character, the physical and mechanical properties of LSAPEs approach those of linear polyethylene.[10−13] This makes PE-18,18 and analogue LSAPEs feasible and sustainable alternatives for classical polyolefins, which are derived from fossil fuels and display poor recyclability. In view of practically relevant material properties, it is necessary to expand studies of crystallization behavior of aliphatic polyesters to include those with longer CH_2 sequences. Herein, we investigate the crystalline morphologies of LSAPEs with CH_2 sequence lengths between consecutive ester groups ranging from 18 to 48.

From the available data, it is known that the ester groups of LSAPEs participate in the crystalline regions, and furthermore, that ester groups act as defects to the crystalline lattice, causing a depression in melting temperature and level of crystallinity relative to that of linear polyethylene.[7] It has also been shown that the crystals of LSAPEs are typically layered, as seen for example in PE-44,5,[10] PE-22,5,[10] PE-22,4,[11] and PE-48,48,[14] among others.[15−20] A crystal structure in which functional groups are present in layers is also characteristic of many polymers with equally spaced moieties placed along a linear methylene backbone, as found in various precision polyethylenes and polyamides.[21] When such moieties are highly interactive, for example, sulfone,[22] carboxylic acid,[23] or amide,[24] the driving force to form a layered crystal structure originates from strong intermolecular functional group interactions, often hydrogen bonding. In precision polyethylenes with weaker interactive functional groups, the layered packing is driven instead by maximizing van der Waals interactions of CH_2 groups and by preferential folding of the polymer chains at or near the substitution, as is the case for precision polyethylenes with halogens.[21,25,26]

For aliphatic polyesters, ester layer packing is expected to be driven by dipole−dipole interactions.[7,27,28] Interactions between the esters of adjacent chains reduce the enthalpic penalty that occurs as a result of incorporating ester groups into the crystal lattice. Despite the presence of the ester groups within crystallites, LSAPEs maintain a polyethylene-like orthorhombic crystal lattice,[11,17,18] meaning that van der Waals interactions between adjacent CH_2 sequences play the major role in determining the drive for crystallization. This will be especially true as the length of the CH_2 sequences is increased, i.e., as the number of ester groups in the polyester chain decreases. The LSAPEs studied here provide the opportunity to probe if structures other than the usual layered one may evolve under different crystallization conditions or modes when the distance between consecutive ester groups increases from 18 to 48 methylenes. PE-48,48 is the longest-spaced polyester synthesized to date,[5] making it a particularly apt candidate for this purpose. Crystalline structures developed under fast cooling from the melt are of special focus in the present study as such processes will mimic those used in commercial production and will thus drive the useful properties of these materials.

EXPERIMENTAL PART

Materials. The synthesis and molar mass characterization of the long-spaced aliphatic polyesters (LSAPEs) studied here have been reported in previous works.[5,9,13] The nomenclature for all LSAPEs is PE-*X*,*Y*, where *X* indicates the number of carbon atoms in the diol and *Y* indicates the number of carbons in the diacid. The structural repeating unit is $-[O-(CH_2)_X-O-(C{=}O)-(CH_2)_{Y-2}-(C{=}O)]_n-$. For the polyesters studied here, $X = Y = 18$, 19, 32, or 48. These PE-*X*,*Y* polyesters are considered pseudo-precise polyethylenes, as the number of CH_2 groups between each ester group alternates between X and $X - 2$.

Relevant chain characteristics are listed in Table SI.1. The weight average molecular weight, M_w, determined using gel permeation chromatography (GPC), ranges between 30 and 90 kg/mol, and all LSAPEs have a polydispersity index (M_w/M_n) of around 2. Thermal properties, including peak crystallization and melting temperatures obtained with differential scanning calorimetry (DSC), are also listed in the table.

Measurements. *Thermal Analysis.* For initial DSC measurements, the original samples were placed between two thin sheets of Teflon and melt pressed to form films of ∼100 μm thickness. Around 4 mg of these films were encapsulated in aluminum DSC pans for thermal analysis. Static temperature, thermal lag, and heat of fusion in the DSC were calibrated with indium, and all operations occurred under dry N_2 flow. The DSC is connected to an RC900 intracooler to allow for subambient temperature control. For thermal characterization, samples were brought to ∼30 °C above the final observed melting temperature and held for 5 min to erase thermal history before cooling and heating at 10 °C/min to observe the crystallization and melting thermograms.

To test the impact of different cooling rates on thermal behavior, samples were cooled from the melt at rates of 5, 10, 20, 40, and 100 °C/min before subsequent heating at 10 °C/min. Although ∼40 °C/min is the limit of cooling for classical DSC in the temperature range used here, a nominal rate of 100 °C/min was included to ensure that the fastest cooling rate possible was achieved. In addition to cooling at different rates inside the DSC, samples were rapidly quenched ex situ, after which they were quickly encapsulated in a DSC pan and heated at 10 °C/min to observe the melting endotherm. The rapid quenching procedure involved sandwiching a sample between two pieces of ∼10 μm aluminum foil (to ensure maximum heat transfer) and bringing it from the melt as quickly as possible into an ice water bath at 0 °C.

Simultaneous Small-Angle X-Ray Scattering (SAXS)/Wide-Angle X-Ray Diffraction (WAXD). A Bruker Nanostar diffractometer with an Incoatec microfocus X-ray source (Iμ*S*) was used to collect simultaneous small-angle X-ray scattering (SAXS) and wide-angle X-ray diffraction (WAXD) patterns at room temperature. The incident X-ray beam was a Cu Kα line with a wavelength λ of 1.5418 Å. The diffractometer was equipped with a HiStar 2D Multiwire SAXS detector and Fuji Photo Film plate for WAXD detection, and the plate was read with a Fuji FLA-7000 scanner.

For X-ray analysis of nonisothermally and isothermally crystallized samples, one piece of the ∼100 μm melt-pressed film was placed inside a DSC pan and either cooled from the melt at 40 °C/min to 25

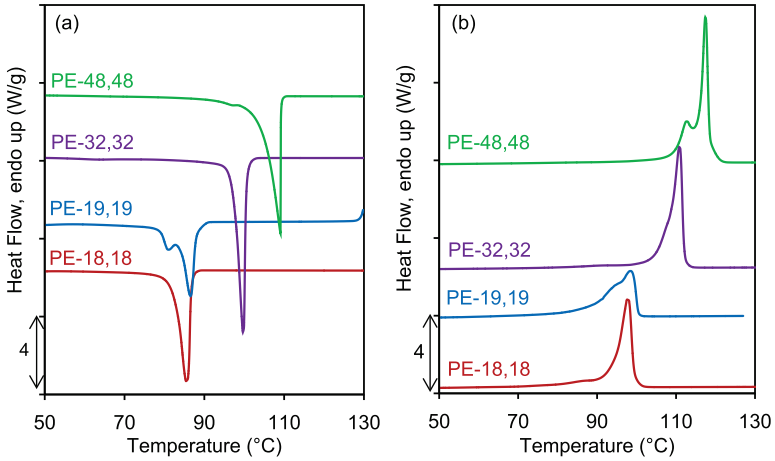

Figure 1. Crystallization exotherms (a) and subsequent melting endotherms (b) of long-spaced aliphatic polyesters PE-18,18 (red), PE-19,19 (blue), PE-32,32 (purple), and PE-48,48 (green) collected by DSC at 10 °C/min. Data have been vertically shifted for clarity.

°C (nonisothermal) or cooled from the melt to the selected isothermal crystallization temperature, T_c, held there for long enough to develop a full exothermic peak and finally cooled at 40 °C/min to 25 °C. The samples were then removed from the DSC pans and brought to the X-rays. Rapidly quenched samples prepared using the method described above were also analyzed by X-rays. In addition to the initial ~100 μm films quenched to 0 °C, thinner films of ~20 μm were also prepared using this rapid quenching method, and quenched from the melt to temperatures ranging between 0 and 100 °C. Either ice or a hot plate was used to control the temperature of the water bath into which the samples were quenched.

A Peltier device placed in the sample holder of the Bruker instrument was used to record X-ray patterns on heating. These in situ temperature variable experiments were carried out with samples quenched to 0 °C. Quickly after rapid quenching, samples were brought to the X-rays and placed inside the sample holder of the Peltier device, which was at a temperature of ~5 °C. SAXS patterns were collected at every 5 °C on heating.

From the WAXD diffractograms, the level of crystallinity X_c was estimated by peak deconvolution, assuming a two-phase (amorphous and crystalline) model. SAXS patterns were Lorentz-corrected to determine the long period L. The long period and crystal thickness were also estimated using the normalized one-dimensional correlation function ($\gamma(r)$) applied to the first-order SAXS peak and obtained as a function of the correlation distance r[29,30]

$$\gamma(r) = \frac{\int_0^\infty I(q)q^2\cos(rq)\mathrm{d}q}{\int_0^\infty I(q)q^2\mathrm{d}q}$$

Appropriate extrapolations at $q \to 0$ and $q \to \infty$ were conducted according to the method described by Goderis[31] and outlined by us previously.[14]

Fourier Transform Infrared (FTIR) Spectroscopy. Spectra were collected at room temperature using a Thermo Scientific Nicolet iS50 spectrometer equipped with a DTGS KBr detector. OMNIC software provided with the instrument was used for operational control and peak analysis. Absorption mode was used in a wavenumber range between 400 and 4000 cm^{-1} with 2 cm^{-1} resolution. Spectra were collected on the ~100 μm polyesters prepared by rapid quenching to either 0 or 80 °C.

Polarized Optical Microscopy (POM). Polarized optical micrographs were obtained using a type BX51 Olympus optical microscope equipped with an Olympus digital CCD camera. CellSens software provided by Olympus was used to analyze the obtained images. For temperature control, we used a Linkam hot stage connected to a TMS94 temperature programmer. Films of ~20 μm thickness were placed between two glass coverslips, heated to ~30 °C above the observed melting temperature, held for 5 min, and rapidly quenched to either 0 or 80 °C using temperature-controlled water baths. Images were collected at room temperature and on heating from room temperature at a rate of 10 °C/min. The same samples and exposure settings were used for both quenching temperatures.

RESULTS AND DISCUSSION

Nonisothermal Crystallization and Melting Behavior. Shown in Figure 1 are crystallization exotherms (a) and subsequent melting endotherms (b) collected by DSC at a rate of 10 °C/min. PE-18,18, PE-32,32, and PE-48,48 crystallize with sharp, single exothermic peaks, while a double exotherm consisting of an initial relatively sharp peak followed by a smaller shoulder at lower temperatures is observed for PE-19,19. The peak crystallization and melting temperatures decrease with the increasing ester content (values are tabulated in Table SI.1). This behavior is consistent with previous work on shorter-spaced LSAPEs of the type PE-*X*,*Y*, where *X* = *Y*,[5,12,20,32,33] as well as other polyethylenes with precisely placed moieties that may be incorporated into the crystalline regions and act as defects decreasing the melting temperature and retarding the crystallization process, including, for instance, halogens,[34] acid,[23] and methyl and ethyl branches.[35,36]

PE-48,48 and PE-19,19 have double melting peaks on heating at 10 °C/min. It was demonstrated in a previous study that the double melting peak of PE-48,48 occurs due to the presence of crystals with the same crystallographic packing but different thicknesses.[14] Specifically, lower and higher melting peaks correspond to crystals with noninteger and integer (3 full layers) numbers of ester−ester layers, respectively. The higher melting temperature of the integer-layered crystals was associated with a decrease in surface free energy due to the placement of the ester moiety at the lamellar basal surface upon completion of the ester layer. We postulate that a similar phenomenon may be the cause of the double melting peak in PE-19,19, while reorganization of an initial noninteger structure to the integer form on melting may be too fast in PE-18,18 and PE-32,32 as the double melting is not as prominent in these samples.

Interestingly, the heat of fusion ΔH_m observed for PE-19,19 is ~10% lower than that of PE-18,18 (see Table SI.1). This apparent anomaly could be explained by the odd−even effect

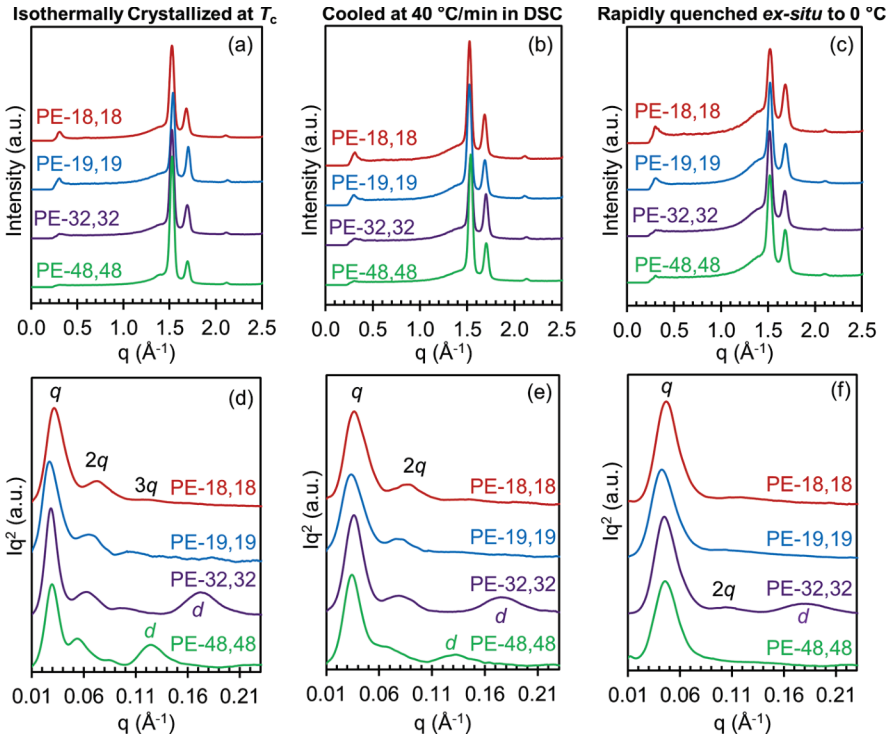

Figure 2. (a–c) WAXD and (d–f) Lorentz-corrected SAXS patterns for PE-18,18 (red), PE-19,19 (blue), PE-32,32 (purple), and PE-48,48 (green) obtained at room temperature after isothermal crystallization (a, d) at T_c = 90, 90, 102, and 110 °C, respectively, cooling from the melt in DSC at 40 °C/min (b, e) and after rapid quenching to T_q = 0 °C in ice water (c, f). *q*, 2*q*, and 3*q* in (d–f) indicate the first-, second-, and third-order long period, respectively, while *d* indicates the ester layer scattering in PE-48,48 and PE-32,32. Data have been vertically shifted for clarity and normalized by their total area for ease of comparison.

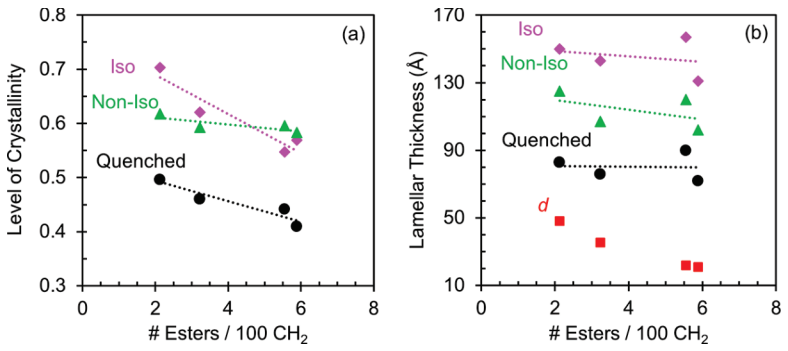

Figure 3. Level of crystallinity (a) and lamellar thickness (b) as a function of the number of ester groups per 100 CH_2 groups for isothermal crystallization (pink diamonds), nonisothermal crystallization (green triangles), and rapid quenching (black circles). Red squares in (b) are the distances corresponding to the observed ester layer reflections.

on thermal properties, which occurs in *n*-alkanes[37,38] and in many molecules with moieties inserted at a precise equal length along a polyethylene backbone.[7,39,40] When the number of CH_2 groups between consecutive ester groups is even and the polymer is in an *all-trans* conformation, the configuration of consecutive carbonyl oxygens (C═O) with respect to the chain backbone alternates, allowing opposing ester dipole moments to cancel out and stabilizing the structure. In contrast, for an odd number of CH_2 groups, the configuration of consecutive carbonyl oxygens in the backbone is maintained, preserving the local polarization and creating a less stable crystal structure.[7] Therefore, although PE-19,19 does have slightly higher T_m and T_c than PE-18,18 (as would be expected in the absence of the odd–even effect), some differences in crystal packing and crystalline properties, including heat of fusion, are expected in odd short-spaced polyesters with respect to even analogues. Clearly, such a known configurational difference explains the odd–even effect observed in polycarbonates in a recent paper.[41] The odd–even effect diminishes with the increasing length of the CH_2 spacer.[7,39]

Isothermally Crystallized, Nonisothermally Crystallized, and Rapidly Quenched LSAPEs. Simultaneously collected SAXS/WAXD measurements were used to investigate the impact of different rates of quenching and quenching depths on the crystalline structure of the series of LSAPEs. Figure 2 shows X-ray patterns collected at room temperature after three crystallization conditions, isothermal crystallization at the T_c listed in the legend, cooling at 40 °C/min in the DSC

from the melt to 20 °C, and very fast manual quenching from the melt into ice water. The WAXD patterns, given in Figure 2a–c, are equivalent to the diffractogram of orthorhombic polyethylene. The two major reflections correspond to the (110) plane at $q \sim 1.53$ and (200) plane at ~1.69 Å^{-1} for all LSAPEs regardless of crystallization conditions. The orthorhombic packing is expected as this unit cell structure has been found in other LSAPEs, including PE-22,5 and PE-44,5,[10] PE-22,4,[11] PE-15,[17] and PE-16.[18] After both isothermal and nonisothermal crystallization, the level of crystallinity obtained from the WAXD patterns is X_c ~60–70%, while on very fast quenching, X_c is reduced by ~10–20% for all LSAPEs, as shown in Figure 3a.

Lorentz-corrected SAXS patterns of isothermally crystallized LSAPEs (Figure 2d) display first- (q), second- ($2q$), and third-order ($3q$) long period scattering, corresponding to highly correlated lamellae stacks. Values of q, $2q$, $3q$, and the corresponding distances are listed in Table SI.2. Other prominent scattering peaks at q ~0.131 and ~0.178 Å^{-1} in Figure 2d are the ester layer (d) reflections for PE-48,48 and PE-32,32, respectively. In other words, the reflection marked as "d" corresponds to the distance between planes formed by the intermolecular staggering of ester groups. The positions of these reflections remain constant irrespective of T_c and correspond reasonably well with the calculated *all-trans* distances between ester groups after accounting for chain tilts of ~38° and 30° for PE-48,48 and PE-32,32, respectively. When the rate of crystallization is increased by cooling at 40 °C/min in DSC from the melt to room temperature, the crystals develop a lower degree of periodicity, as shown by the absence of $3q$ in Figure 2e. The core lamellar thickness l_c estimated from the normalized one-dimensional correlation function (CF), applied to q, is ~30–50 Å lower after nonisothermal crystallization when compared to the isothermal values, as depicted in Figure 3b. Hence, the increased undercooling on nonisothermal crystallization leads to thinner crystals as expected, while X_c remains basically unchanged. Values of X_c, l_c, and the linear crystallinity, ϕ, (level of crystallinity within the lamellae stack cluster, for example, within a spherulite, calculated from the CF[31,39]) are tabulated in Table SI.3.

Decreasing the crystallization temperature further by rapidly quenching the polyesters from the melt to 0 °C results in a deeper loss of correlated lamellae stacking, evident by the disappearance of the $2q$ reflections in most of the patterns and the loss of the d reflection in the SAXS pattern of PE-48,48 (Figure 2f). Although not vanished, the magnitude of the corresponding second-order reflections and d spacing in PE-32,32 are greatly reduced as well. Note that the layer reflections of PE-19,19 and PE-18,18 correspond to $q > 0.25$ Å^{-1} and are beyond our SAXS detection limit. Additionally, a faster rate of quenching results in dramatically reduced X_c, and l_c; the latter being nearly 50% lower than after isothermal crystallization (see Figure 3b). Despite the significant depletion of long-range order and periodicity under rapid quenching to 0 °C, the orthorhombic unit cell is maintained (Figure 2c).

The correlated crystalline ester layer reflections for PE-19,19 and PE-18,18 can be observed in the lowest q region of the WAXD patterns, as seen in Figure 2a,b. Unfortunately, the first layer reflection overlaps at low q with scattering from the opening of the diffraction plate. A more intense reflection at $q \sim 0.3$ Å^{-1} in the WAXD patterns of PE-19,19 and PE-18,18 compared with the other two polyesters confirms additional scattering from the first ester layer, as is highlighted in Figure SI.1. After isothermal crystallization, PE-19,19 and PE-18,18 both display first- (d) and second-order ($2d$) ester layer reflections. The $2d$ reflections are not affected by the plate opening and, therefore, may be used to calculate the layer distance in both PE-19,19 and PE-18,18 (Table 1).

Table 1. Ester Layer Distance and Chain Tilt in Long-Spaced Aliphatic Polyesters[a]

sample	all-trans[b] repeat length (Å)	observed layer distance, d (Å)	tilt angle[c] (±1°)
PE-18,18	22.9	20.8 ± 0.2[d]	25
PE-19,19	24.1	21.8 ± 0.2[d]	25
PE-32,32	40.6	35.3 ± 0.5[e]	30
PE-48,48	60.9	48.0 ± 0.6[e]	38

[a]Samples crystallized isothermally or cooled at 40 °C/min in DSC. [b]Calculated with all-trans C–C distance of 1.27 Å and C–O distance of 1.17 Å. [c]Estimated chain tilt with respect to the lamellar normal assuming an all-trans structure. [d]Second-order layer observed in WAXD (Figure SI.1). [e]First order observed by SAXS (Figure 2).

Furthermore, the presence of ester layers was confirmed from synchrotron patterns collected at Argonne National Laboratory on samples cooled to room temperature, see Figure SI.2. The $2d$ reflections are not observed in PE-19,19 and PE-18,18 on rapid quenching, as shown in Figure SI.1b, a behavior analogous to that observed for PE-48,48 and PE-32,32 under the same fast crystallization to 0 °C.

Ester layer distances and calculated tilt angles between the chain and layer normal are tabulated in Table 1. The calculated tilt angles, between 25 and 38°, are in line with values found for other LSAPEs,[11] polyethylenes, and *n*-alkanes,[42,43] as well as precision polyethylenes with halogens.[25,26] It has been proven that the chain tilts with respect to the layer normal to reduce overcrowding and an anomalous density increase at the surface of the lamellae.[42] Under isothermal crystallization at low undercooling, the lamellae of the LSAPEs studied comprise an integer number of ester repeats, with the ester groups at the basal surfaces and contributing to the chain tilt.

Although for polyethylenes, the chain tilt angle increases with increasing molecular weight,[42,43] the variation of chain tilt of LSAPEs scales with the length of the methylene spacer rather than with molecular weight. This trend may result from conformational disorder around the two CH_2 adjacent to the ester group.[25,26] We expect the tendency to deviate from the all-trans packing of LSAPEs to increase with the number of layers in the crystal as the ester content in the chain increases, and thus alleviate some of the need for the chain to tilt to reduce the excess density at the lamellar surface.

The presence of ester layer reflections after relatively slow crystallization conditions is expected since layered crystallites have been found previously in other aliphatic polyesters,[10,11,15–20] and furthermore in most precision polyethylenes.[22,25,26,39,44–46] However, the reduction in ester layer periodicity after rapid quenching for PE-32,32, PE-19,19, and PE-18,18, and especially the complete disappearance of the layer reflection in PE-48,48 is quite remarkable, since all other reported fast quenched systems have been found to be layered. Even the recently studied long-spaced polyacetals that adopt a disordered, mesomorphic-like structure under fast crystallization were found to be layered.[39,40,47]

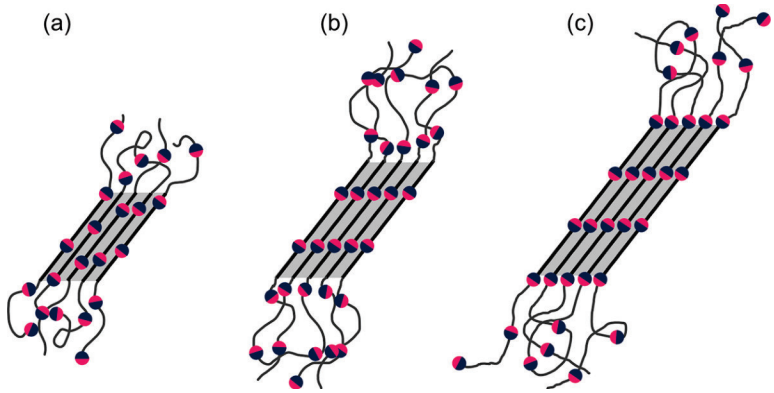

Figure 4. Schematic diagrams for (a) unlayered crystals formed under rapid quenching to 0 °C, (b) noninteger-layered crystals formed on quenching inside the DSC, and (c) integer-layered crystal structures of LSAPEs formed under isothermal crystallization. Circles represent ester groups, where pink and blue indicate −(C═O)− and −O−, respectively.

The fact that no layer reflection is evident in PE-48,48 on rapid quenching indicates one of two structural possibilities. Either the core lamellae thickness, l_c, under these crystallization conditions is less than the all-trans distance between consecutive esters and the ester groups remain in the amorphous region or the ester groups reside inside the crystals but are not layered. As shown in Figure 3b, the l_c of all rapidly quenched LSAPEs are considerably larger than d and larger than the all-trans ester−ester distances listed in Table 1. For example, for rapidly quenched PE-48,48, the l_c is ∼83 Å, compared to d = 48.0 Å and to the theoretical ester−ester distance of 60.9 Å. Such difference is accentuated in the shorter LSAPEs. Thus, the core crystal accommodates the ester units, which under these fast crystallization conditions must be randomly dispersed or unlayered, as illustrated schematically in Figure 4a. Schematics are also given for noninteger-layered crystals that develop by cooling from the melt in the DSC (Figure 4b) and for integer-layered crystallites that form under isothermal crystallization (Figure 4c).[14] Note that the number of ester groups per crystallite shown in Figure 4 is reflective of the structure of PE-48,48, but the general features of the schematics apply as well to the shorter LSAPEs. The ratio (l_c/d) for unlayered crystals or the number of ester layers in the core-layered crystals is listed in Table SI.3 for each LSAPE.

The possibility of unlayered packing of functional or pendant groups precisely placed on a polyethylene backbone was postulated in a 2015 review;[21] however, to the best of our knowledge, the data on PE-48,48 represent the first clear evidence of the formation of unlayered crystallites on fast quenching from the melt. Notable is the fact that both layered and unlayered structures are accessible in PE-48,48 depending on the rate and depth of quenching.

The impact of the cooling rate on the crystal structure of semicrystalline polymers has been widely studied in many systems. In general, when rapid cooling rates are applied, a lower degree of crystal ordering is expected. Often, different rates of cooling result in different polymorphic structures, but a change from a layered to an unlayered crystalline structure with the increased cooling rate is unprecedented. For instance, it is well known that highly isotactic polypropylene (iPP) forms a mesomorphic structure on rapid cooling from the melt and a monoclinic phase under slower crystallizations.[48,49] Similarly, mesomorphic forms were found recently in fast quenched long-spaced polyacetals.[39,47] Other common polymers, such as syndiotactic polystyrene,[50] polyamide 66,[51] and polyamide 6,[52] also form different polymorphs depending on the rate of cooling. In contrast, for a series of polyhydroxyalkanoates, the lamellar thickness and spherulitic morphologies were highly dependent on the cooling rate, but the crystal structure remained unchanged.[53]

The reduction in X_c and l_c on rapid quenching in PE-32,32, PE-19,19, and PE-18,18 is analogous to the behavior of PE-48,48. Furthermore, the disappearance of both $2q$ and $2d$ in PE-19,19 and PE-18,18 (Figure SI.1), along with the large reduction in $2q$ and d reflections of PE-32,32, indicate that rapid quenching to 0 °C partially impedes the ability of these shorter-spaced polyesters to pack into the highly symmetric layered structures, which occur on slower crystallization. As $2q$ is also lost for quenched unlayered PE-48,48, we posit that a mixture of layered and unlayered crystallites is formed in polyesters shorter than PE-48,48 under the same rapid quenching.

The mixed unlayered and layered crystals on rapid quenching to 0 °C in PE-32,32, PE-19,19, and PE-18,18 are explained on the basis of a number of crystalline layers found in the crystals of these polyesters compared to those found in the PE-48,48 crystallites. As seen in Figure 3b, under fast quenching to 0 °C, the crystal thickness is 80 ± 5 Å for all polyesters. Since 80 Å corresponds to ∼4 repeating units of the two shortest-spaced polyesters, even on rapid quenching of these LSAPEs, it is likely that in a fraction of the crystals formed, the esters will end up aligned in layers. Conversely, ester layering is less likely in the crystals of the longer spaced PE-48,48 because only 1.7 repeats are found on average in the chain axis of the crystal (see Table SI.3). It is thus concluded that two factors play a role in the formation of unlayered crystalline structures of LSAPEs: the distance between consecutive functional groups and fast cooling rates analogous to those used in industrial melt processes.

Dependence of the Crystalline Structure on the Depth of Quenching. With a focus on rapid quenching, in this section, we investigate the quenching temperature T_q at which a layered structure is recovered either by the appearance of d or $2q$ with increasing T_q. Figure 5a−c show Lorentz-corrected SAXS patterns for PE-48,48 (a), PE-32,32 (b), and PE-18,18 (c) as a function of increasing quenching temperatures T_q ranging from 0 to 100 °C. Note that the X-ray patterns were collected at room temperature for thin films

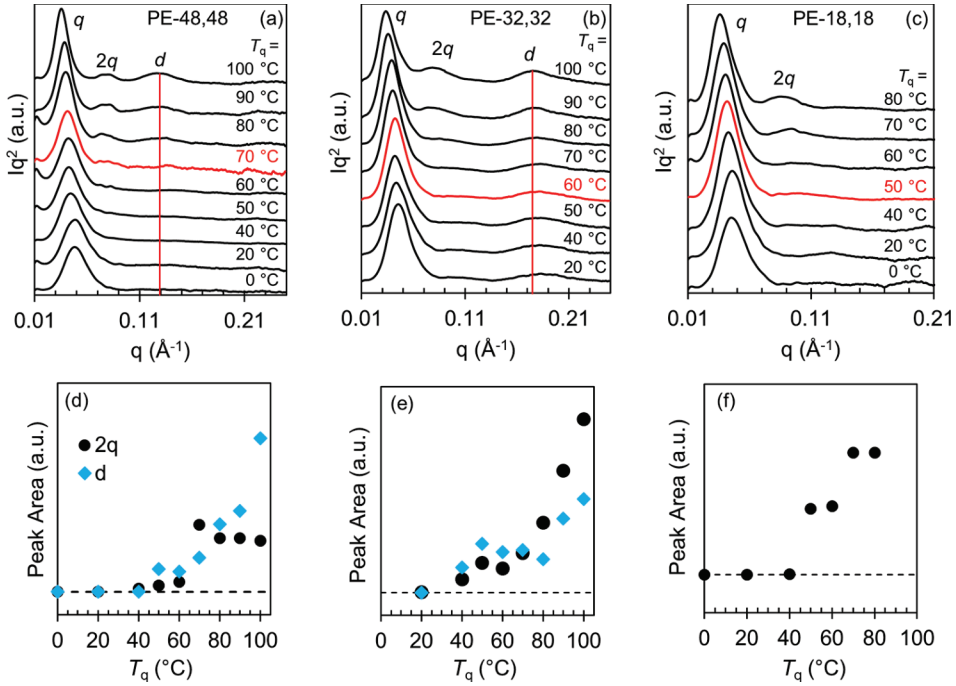

Figure 5. (a–c) Lorentz-corrected SAXS patterns of PE-48,48, PE-32,32, and PE-18,18 collected at room temperature after rapid quenching to the indicated temperatures. The red vertical lines denote the location of the ester layer scattering for PE-48,48 and PE-32,32. Data have been normalized by area and shifted vertically for clarity. Red patterns in (a–c) indicate the T_q at which the 2q and/or d scattering is first observed. (d–f) Area of the 2q peak (black circles) and d (blue diamonds) peak for the patterns shown in (a–c) relative to that at T_q = 0 or 20 °C.

(~20 μm) that were melted under two hot plates and very quickly quenched in a water bath held at the temperatures indicated.

In Figure 5d–f, the areas of the 2q and d peaks are quantified relative to their values at T_q = 0 or 20 °C. The red vertical lines in the figure demarcate the layer reflection. For PE-48,48, rapid quenching up to $T_q \leq$ 60 °C results in X-ray patterns with no 2q or d periodicity, indicating the formation of the unlayered structure. Concomitant with the formation of the layered structure at T_q > 60 °C, the areas of the 2q and d reflections display a sudden increase. As both the 2q and d reflections become visible at the same T_q, we conclude that the onset of 2q is indeed correlated with the formation of a more correlated lamellar-layered crystal structure.

Since for shorter-spaced polyesters, layered and unlayered crystals coexist even after fast quenching, we focus on the evolution of 2q with increasing T_q to evaluate the onset of unlayered crystals for these polyesters. For PE-32,32, 2q starts to increase at T_q between 50 and 60 °C, as seen in Figure 5e, and a similar increase is observed for PE-18,18 in Figure 5f, demarcating the transition from mixed to all layered crystals. The 2d reflection is not apparent in any of the WAXD patterns for PE-18,18, regardless of T_q (Figure SI.3). The data in Figure 5 indicate a tendency for the transition temperature from the unlayered to layered structure to increase from 50 °C to 70 °C with an increasing methylene spacer. In summary, the trends with the temperature, as shown in Figure 5d–f, confirm that polyesters spaced by ≥ 18 methylene groups develop unlayered crystals under fast quenching to T_q < ~50 °C and that >32 CH_2 spacing is needed for the formation of a completely unlayered structure.

The variation of the WAXD level of crystallinity (X_c) and the crystal thickness (l_c) calculated from the q data of Figure 5 shows a small and gradual increase with T_q (Figure SI.4). A sudden increase of X_c or l_c at the transition temperature between unlayered and layered structures is not observed.

Morphology of Rapidly Quenched LSAPEs. To further probe the impact of the depth of quenching on the crystallization of the LSAPEs, we employed polarized optical microscopy (POM) to contrast the morphology after rapid quenching at temperatures below and above the unlayered–layered transition. Figure 6 displays room temperature micrographs for PE-18,18 (top), PE-32,32 (middle), and PE-48,48 (bottom) after rapid quenching to T_q = 0 °C (left) and T_q = 80 °C (right, 70 °C for PE-18,18). Note that for all polyesters, unlayered crystals are expected on rapid quenching to T_q = 0 °C, while layered crystals are expected at the higher T_q (see Figure 5a–c). The same film was used for both quenching modes.

Regardless of T_q, rapid quenching of the studied polyesters leads to a highly nucleated, spherulitic morphology, as seen in all images. The major difference between the two quenching modes is the brightness of the micrographs. As expected for crystallization at a higher undercooling, nucleation is much more profuse for rapid quenching to low T_q than to high T_q. Hence, smaller spherulites and a lower level of crystallinity (Figure SI.4) result in a dramatic decrease of birefringence in the images of LSAPEs quenched to 0 °C. In comparison, the lower nucleation density of the polyesters quenched to 70 or 80 °C leads to larger, brighter spherulites and a coarser overall morphology. The birefringence of the LSAPEs quenched at high temperatures may also be accentuated by the intrinsic increase in symmetry of the layered crystalline structure. Therefore, these POM images further support the layered and unlayered core lamellar morphology, in agreement with the SAXS data discussed above.

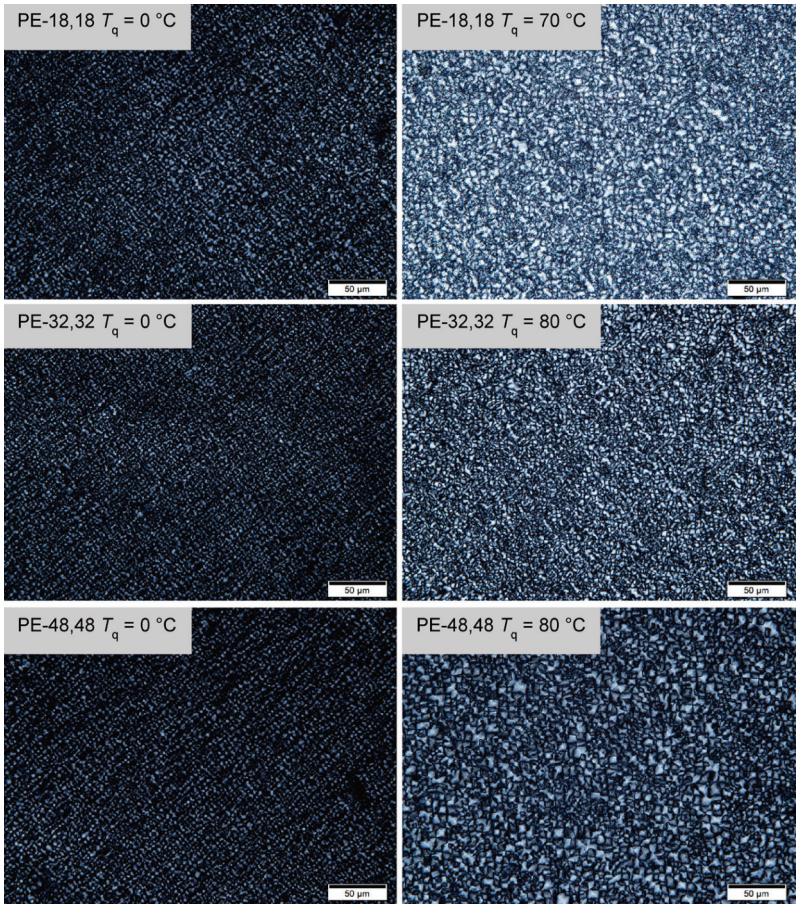

Figure 6. Polarized optical micrographs for PE-18,18 (top), PE-32,32 (middle), and PE-48,48 (bottom) prepared by rapid quenching to T_q = 0 °C (left) or 70 or 80 °C (right) between two glass slides. The same samples and exposure settings were used for quenching at both temperatures. Scale bars are 50 μm.

Melting Behavior of Unlayered and Layered Polyesters. To investigate differences in melting between unlayered and layered structures, all LSAPEs were first rapidly quenched ex situ at 0 °C, quickly encapsulated, and placed in the DSC sample cell. The temperature was lowered to −20 or to −50 °C prior to recording melting. After the first melting, the samples were subsequently cooled at a nominal rate of 100 °C/min (to ensure the fastest rate possible in classical DSC) to the same low temperature and melted again to compare the results. Note that from Figure 2, recrystallization inside the DSC leads to layered crystals even at the fastest DSC cooling rate.

Melting endotherms collected after both quenching conditions are shown in Figure 7. All four polyesters quenched quickly outside the DSC (solid lines in Figure 7) display a low-enthalpy endothermic transition over a broad range of temperatures (from ∼25 to 60 °C), which can be seen in the zoomed-in perspective of Figure 7b. In contrast, the melting curves of LSAPEs cooled at 100 °C/min inside the DSC (dashed lines in Figure 7) do not show any of this low-temperature transition. The end of the low-temperature endothermic event is about 60 ± 10 °C, which coincides with the temperature at which layered crystallites start to develop on cooling directly from the melt (Figure 5); therefore, we associate the shallow low-temperature transition with a transformation on heating from unlayered to layered crystallites.

Although we cannot rule out that the transformation could occur via melting recrystallization, it is likely that on fast quenching, a metastable unlayered structure with a higher free energy forms. The increased thermal motion on heating allows sliding along the chain axis until the ester groups stagger into the thermodynamically more stable layered structure. The latter is supported by micrographs shown in Figure SI.5, which demonstrate no visual evidence of melting recrystallization taking place during heating of rapidly quenched samples at temperatures below the main melting event. The only morphological change that occurs on heating is a slight increase in the birefringence, indicating increased symmetry in the lamellar structure, in support of a transformation from unlayered crystals to the layered type upon heating.

The similarity between the thermal behavior of rapidly quenched PE-48,48 and the shorter-spaced polyesters further confirms the formation of the unlayered form in PE-32,32, PE-19,19, and PE-18,18. In all cases, ΔH_m after rapid quenching is ∼10−15% lower than the ΔH_m observed after cooling at a nominal rate of 100 °C/min. This result infers that even after transformation on heating, the level of crystallinity is lower than for layered crystals formed on quenching in the DSC, which is consistent with the lower level of crystallinity

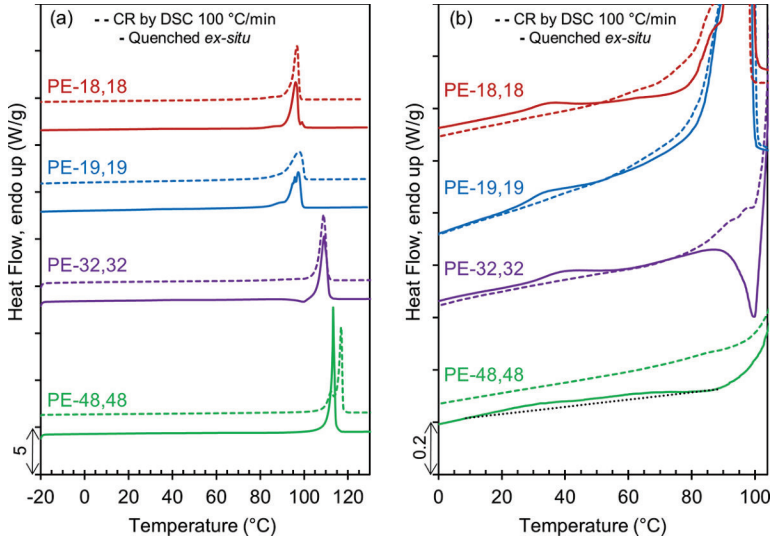

Figure 7. DSC melting endotherms for PE-48,48 (green), PE-32,32 (purple), PE-19,19 (blue), and PE-18,18 (red) after cooling by DSC at 100 °C/min (dashed lines) and after rapid ex situ quenching into water at 0 °C (20 °C for PE-48,48). (b) is a zoomed-in perspective of (a). Data have been vertically shifted for clarity, and the black dotted line is added to the PE-48,48 endotherm collected after rapid quenching in (b) to help guide the eye over a broad, shallow transition.

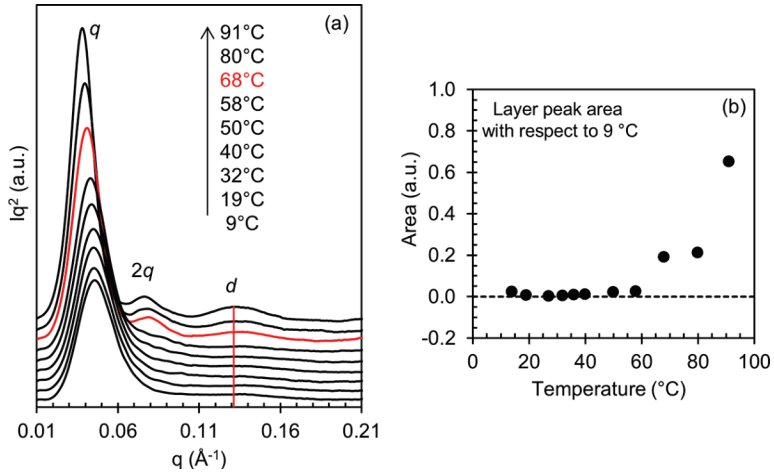

Figure 8. (a) In situ Lorentz-corrected SAXS patterns collected at the indicated temperatures upon heating an unlayered sample of PE-48,48, which was fast quenched to 0 °C. The temperature at which the layer peak is clearly demarcated is shown in red, while the location of the ester layer peak, *d*, is indicated by the red, vertical line. Data have been shifted vertically for clarity. (b) Quantification of the area of the ester layer peak as a function of temperature.

observed via WAXD after manual rapid quenching than after cooling in the DSC (Figure 3a).

The high-temperature double melting peak observed in Figure 7 for PE-48,48 after cooling within the DSC (see Figure 1b for a more clear visual) is associated with the melting of noninteger (lowest melting peak) and integer-layered crystals (highest melting peak), as discussed in a prior work.[14] On heating after rapid quenching, it is clear in Figure 7 that only the lowest melting peak is present, indicating that unlayered PE-48,48 crystals heated to temperatures >60 °C transform into the noninteger-layered structure. Given that metastable noninteger PE-48,48 crystals require relatively long isothermal annealing to thicken to layered crystals of integer thickness,[14] it is not surprising that relatively fast heating at 10 °C/min, as used in Figure 7, is insufficient to form the most thermally stable crystallites for PE-48,48. This feature is less evident in the shorter-spaced polyesters where, upon transformation, crystals melt at the same temperature of the layered form. The data of Table SI.3 suggest that as the spacing between esters is reduced, integer-layered lamellar crystals flanked by ester groups at the basal surfaces are favored even under mild quenching from the melt and on transformation of the unlayered into layered crystals on heating.

It must be emphasized that the fastest cooling rate possible using classical DSC does not replicate the process of crystallization on rapid ex situ quenching (Figure 2). In fact, the crystallization temperature in general changes very little (≤2 °C) even when the cooling rate is increased from the standard 10 °C/min to a nominal rate of 40 °C/min or higher (see Figure SI.6). Thus, the question becomes how fast must we cool to observe the unlayered phase. To overcome the limits of classical DSC, fast scanning calorimetry (FSC) was

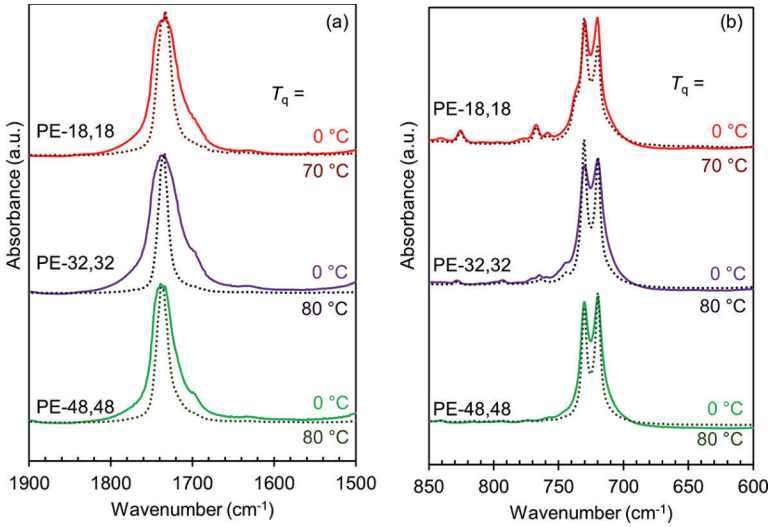

Figure 9. Room temperature FTIR spectra collected after rapid quenching to the indicated temperatures for PE-18,18 (red), PE-32,32 (purple), and PE-48,48 (green) within the regions of C═O stretching (a) and CH_2 rocking (b). T_q = 0 °C produces unlayered crystals (shown in lighter colors), T_q = 70 or 80 °C produces layered crystals (shown as dotted lines in darker colors). Data have been normalized by the height of the band at 1740 cm^{-1} in the region from 1900 to 1500 cm^{-1} (a) and by the height of the band at 720 cm^{-1} in the region 850−600 cm^{-1} (b). Vertical shifting is done for clarity.

employed in an attempt to answer this question. With FSC, extremely fast cooling and heating rates are possible due to the small sample mass used (Figure SI.7). However, even on cooling at rates of 4000 K/s, the formation of the layered structure was not bypassed (Figure SI.8). The crystallization peak was found above the transition temperature. Hence, it is not possible to replicate the results of ex situ quenching using FSC. Manually fast quenching a relatively thin sample from the melt is the most effective route to form the unlayered structure in the LSAPEs.

Transformation from Unlayered to Layered Structure on Heating. The transformation from the unlayered to the layered structure on heating was investigated in the two longest-spaced polyesters by collecting SAXS patterns during heating of unlayered samples obtained by rapid quenching from the melt to 0 °C. Selected Lorentz-corrected SAXS patterns collected in situ on heating PE-48,48 are shown in Figure 8 as a function of increasing temperature; similar patterns for PE-32,32 are given in Figure SI.9. On heating from 9 to 58 °C, no changes are apparent other than a small increase in the long period of about 10 Å. At 68 °C (red pattern in Figure 8a), the $2q$ and d reflections are clearly demarcated, indicating the inception of the layered form, and hence the transformation from unlayered to layered crystals, at temperatures between 58 and 68 °C, in agreement with DSC and prior X-ray data on quenched samples. The integrated area of the d reflection relative to the pattern at 9 °C as a function of temperature (Figure 8b) confirms that the ester layer structure evolves at T > 60 °C. The simultaneous appearance of $2q$ and d reflections at 60 °C < T < 70 °C is equivalent to the data obtained for ex situ quenched samples of PE-48,48 (Figure 5a). The latter reflects the same temperature range for the formation of layered crystals either by fast cooling from the melt or by heating the unlayered structure. Furthermore, the lamellar structural details, such as variation of long period and crystal thickness as a function of temperature, obtained by the CF for the ex situ quenched samples and in situ on heating are also identical (Figure SI.10).

With the discovery that unlayered structures develop in LSAPEs under fast quenching conditions, the next question to address is how stable these structures are at temperatures below their transformation: in other words, whether the unlayered phase will transform into the layered structure at temperatures above the initial T_q but below ~60 °C. To this aim, unlayered PE-48,48 and PE-18,18 were annealed at 40 °C for increasing time up to 35 days, and SAXS/WAXD patterns (Figure SI.11) were obtained at various time points. There is a relatively fast partial transformation within the first annealing day but remains basically unchanged with increasing annealing time. In other words, a significant transformation into the layered phase is not observed. It is therefore concluded that while the transformation of the metastable unlayered structure begins at relatively low temperatures, as shown by the wide shallow low-temperature endotherms of Figure 7, it is only at temperatures ~60 °C approaching the high range of the endotherm when motion and chain diffusion increase for the transformation to be fully completed.

Ester Group Interactions in Unlayered and Layered Crystals. To probe for differences of interactions between ester groups in unlayered and layered crystals, room temperature FTIR spectra were collected on films of constant thickness prepared by rapid quenching to 0 or 80 °C (70 °C for PE-18,18). In Figure 9, the C═O stretching (a) and CH_2 rocking (b) regions of the spectra are shown for PE-18,18, PE-32,32, and PE-48,48. From Figure 9a, LSAPEs rapidly quenched to 0 °C (unlayered crystals, see Figure 5) show a much broader absorbance band for C═O stretching than for the polyesters quenched to the higher temperature (layered crystals). This broadening effect indicates that the C═O groups are present in a greater number of chemical environments after quenching to 0 °C than 70 or 80 °C, which is consistent with the notion that the ester groups are present at random locations within crystallites upon rapid quenching to 0 °C.

To demonstrate that the broadening of the C═O stretching band is not due to differences in the level of crystallinity

between unlayered and layered crystals, we turn to the CH_2 rocking band located at wavenumbers between ~750 and 700 cm^{-1} as shown in Figure 9b. In the case of crystallinity differences, we would expect consistent broadening behavior between the C═O stretching and CH_2 rocking bands. The CH_2 rocking band displays the well-known Davydov splitting effect, which is indicative of the splitting field by the two molecules in the orthorhombic unit cell of polyethylenes and *n*-alkanes.[54,55] After peak deconvolution (see Figure SI.12 for a representative example and Table SI.4 for quantitative band width data), the CH_2 rocking bands at 730 and 720 cm^{-1}, shown in Figure 9b, both have nearly constant width for each LSAPE regardless of T_q. Furthermore, there are no observable changes with T_q in the wavenumber of any of the CH_2 rocking progression modes in the range of frequencies of 720−950 cm^{-1}, assigned using the method developed by Snyder.[55,56] Therefore, differences in the level of crystallinity between unlayered and layered crystals are not the cause of broadening in the C═O stretching band; rather, the observed broadening must be due to differences in the strength and number of interchain ester group interactions. The fact that all LSAPEs show equivalent broadening behavior of the C═O band provides further evidence that rapid quenching induces the formation of unlayered crystals in PE-48,48 and in the shorter-spaced polyesters.

Herein, we have demonstrated that LSAPEs have the ability to pack in layered or unlayered crystalline lamellae, where the ester groups, placed at equal distances along the polyethylene backbone, are either in layers or are randomly arranged inside the crystallites. The formation of layered or unlayered lamellae is controlled by the rate and depth of quenching. LSAPEs must in general be fast quenched to temperatures below ~50−70 °C (depending on the CH_2 spacer length) to develop unlayered structures, while on slower crystallizations, layered crystallites are formed. It is known already that the ester groups of LSAPEs act as defects to the crystalline structure and that interactions between the ester groups of adjacent chains reduce the enthalpic penalty associated with the incorporation of the ester groups into the crystalline lamellae.[7] For instance, layered PE-26,26 has a melting temperature of 114 °C,[12] while the random polyester with an equivalent ester content melts at 107 °C.[57] In unlayered crystals, ester−ester interactions are limited/absent; thus, the structure is less thermally stable than the layered one. The rapid quenching required to form unlayered crystals in LSAPEs, which also inherently reduces l_c, contributes to the observed low transition temperature of unlayered to layered crystals.

In addition to changes in thermal properties, the distribution of the ester groups in LSAPE crystals is expected to impact the mechanical properties of unlayered materials compared to the layered counterparts. For instance, in a set of PCL and PPDL random copolymers, the irregular ester stacking that occurs with increasing content of PCL increases the mobility of the crystalline phase, which in turn lowers the yield stress of the associated copolymer.[58] Furthermore, lower crystallinity usually leads to higher percent elongation. Although mechanical testing is not yet available for the LSAPEs studied here, we expect similar trends when contrasting the properties of unlayered and layered polyesters. Changes in mechanical properties between the unlayered and layered structures may also be accompanied by changes in degradability and/or recyclability of these LSAPEs.

Based on the results presented here, the question becomes how general the development of unlayered crystallites is for the large variety of precision polyethylenes that have been synthesized; and further, if the formation of unlayered structures is directly correlated with the length of the CH_2 sequence between each precisely placed moiety, as it seems to be for the LSAPEs studied here. A review of available literature data is inconclusive on this matter for a number of reasons. First, data reported for newly synthesized precision polyethylenes often do not report any crystal structure analysis.[59,60] Even when some structural information is reported, for example, an X-ray pattern, the range of scattering angles shown is often insufficient to indicate whether the crystals are layered. This has been the case for many recently studied polyesters.[20,61,62] While general X-ray patterns are usually described, longer-range structural details are most often not considered. Furthermore, the crystalline structure is rarely reported for different quenching or different crystallization conditions as those covered in this work.

Despite the abundance of LSAPEs synthesized,[7] there exist very few studies of their crystallization behavior. For instance, LSAPEs PE-25,25[32] and PE-30,30[63] have been synthesized, but efforts to discern their crystalline structure have not yet been undertaken. Similarly, crystallization studies of PE-26,26 thus far include only a single WAXD pattern.[20] Asymmetric LSAPEs including PE-38,23 and PE-44,23[12] along with PE-38,26 and PE-44,26[64] have also been synthesized, but their crystalline properties are yet unknown. We have presented here what is, to the best of our knowledge, the first detailed study of the crystalline morphologies of LSAPEs as a function of both the CH_2 spacer length and crystallization conditions. We demonstrate that uncommon unlayered structures are enabled under very fast quenching from the melt. Such structures are of interest with regard to the processing of these polymers.[9]

CONCLUSIONS

Under rapid quenching conditions, long-spaced aliphatic polyesters with methylene sequence lengths ranging from 18 to 48 between consecutive ester groups form a crystalline lamellar structure of relatively low symmetry. For slower crystallization conditions, i.e., nonisothermal or isothermal crystallization, the crystal structure is much more symmetric, leading to second, or even third, order long period scattering peaks. The expected orthorhombic, polyethylene-like unit cell is maintained regardless of crystallization conditions.

In PE-48,48, SAXS results clearly demonstrate the vanishing of the ester−ester layer peak on rapid quenching, indicating that the lower symmetry crystal structure contains ester groups that are unlayered. Though less clear in PE-32,32 and PE-18,18, structural, thermal, and morphological behavior, which are similar to PE-48,48, demonstrates that the lower symmetry structure of these shorter-spaced aliphatic polyesters contains a fraction of crystallites that are unlayered and a fraction of crystallites that are layered. Layered and unlayered structures are characterized by large differences in melting and reorganization on heating. The crystal thickness and the level of crystallinity are also reduced on rapid quenching by ~50 and 20%, respectively.

On heating of the unlayered phase, transformation into the more symmetric, layered structure is evident both through DSC by a shallow, broad endothermic transition and through in situ SAXS by the appearance of the layer and second-order

long period peaks at temperatures ~60 °C. Only small changes to the crystal structure occur on annealing at 40 °C for over 1 month, indicating a relative stability of the unlayered phase at this temperature.

The unquestionable formation of metastable unlayered crystallites by fast quenching is relevant since industrial processes utilize very fast solidification from the melt. It has already been demonstrated that the tensile properties of LSAPEs match those of commercial polyethylenes while having the advantage of being chemically recyclable at >95% yield.[9] For this reason, and since their monomers are biosourced, LSAPEs have obvious advantages over commercial polyethylenes for single-use disposable products. The transformation of the rapidly formed unlayered structure into the more stable layered form upon annealing at a relatively low temperature (~60 °C) is an additional processing feature to consider in establishing critical structure−property relations of these polyethylene-like materials. When available, similar studies in other linear polymers with regularly spaced moieties will allow for the expansion of our understanding of the role that a very low concentration of in-chain functional groups plays on crystalline morphologies that develop in these systems at high undercooling.

■ ASSOCIATED CONTENT

Molar mass and thermal characteristics of LSAPEs; SAXS peak locations/distances of LSAPEs under different crystallization conditions; lamellar structural details of LSAPEs under different crystallization conditions; low q region of WAXD for PE-18,18 and PE-19,19; MAXS patterns from Argonne National Laboratory for LSAPEs; WAXD for rapidly quenched LSAPEs; X_c and l_c for quenched LSAPEs; unchanged POM of rapidly quenched LSAPEs on heating; thermograms for varying the cooling rate of LSAPEs by DSC; image of PE-18,18 on the FSC sensor; thermograms for varying cooling rate of LSAPEs by FSC; in situ SAXS patterns for rapidly quenched PE-32,32 on heating; comparison of ex situ and in situ structural details on heating rapidly quenched PE-48,48; SAXS/WAXD patterns of unlayered polyesters upon annealing at 40 °C; peak deconvolution of CH_2 rocking band by FTIR (PDF)

■ AUTHOR INFORMATION

Corresponding Author

Rufina G. Alamo − *Department of Chemical and Biomedical Engineering, FAMU-FSU College of Engineering, Tallahassee, Florida 32310, United States;* orcid.org/0000-0002-3061-499X; Email: alamo@eng.fsu.edu

Authors

Stephanie F. Marxsen − *Department of Chemical and Biomedical Engineering, FAMU-FSU College of Engineering, Tallahassee, Florida 32310, United States*

Manuel Häußler − *Department of Chemistry, University of Konstanz, 78457 Konstanz, Germany*

Stefan Mecking − *Department of Chemistry, University of Konstanz, 78457 Konstanz, Germany;* orcid.org/0000-0002-6618-6659

Notes

The authors declare no competing financial interest.

■ ACKNOWLEDGMENTS

Funding of this work by the National Science Foundation, Polymer Program DMR 1607786, is gratefully acknowledged. The authors are indebted to the High Performance Materials Institute of Florida State University for access to X-ray instrumentation and the Advanced Photon Source (APS) at Argonne National Laboratory for synchrotron X-ray data. The authors thank Dr. Theo Siegrist and Masoud Mardani for their help with additional X-ray experiments. M.H. and S.M. acknowledge financial support by the Baden-Württemberg Foundation.

■ REFERENCES

(1) Zheng, Y.; Pan, P. Crystallization of Biodegradable and Biobased Polyesters: Polymorphism, Cocrystallization, and Structure-Property Relationship. *Prog. Polym. Sci.* **2020**, *109*, No. 101291.

(2) Tian, H.; Tang, Z.; Zhuang, X.; Chen, X.; Jing, X. Biodegradable Synthetic Polymers: Preparation, Functionalization and Biomedical Application. *Prog. Polym. Sci.* **2012**, *37*, 237−280.

(3) Vilela, C.; Sousa, A. F.; Fonseca, A. C.; Serra, A. C.; Coelho, J. F. J.; Freire, C. S. R.; Silvestre, A. J. D. The Quest for Sustainable Polyesters − Insights into the Future. *Polym. Chem.* **2014**, *5*, 3119−3141.

(4) Miller, S. A. Sustainable Polymers: Opportunities for the Next Decade. *ACS Macro Lett.* **2013**, *2*, 550−554.

(5) Witt, T.; Häußler, M.; Kulpa, S.; Mecking, S. Chain Multiplication of Fatty Acids to Precise Telechelic Polyethylene. *Angew. Chem., Int. Ed.* **2017**, *56*, 7589−7594.

(6) Chandra, R.; Rustgi, R. Biodegradable Polymers. *Prog. Polym. Sci.* **1998**, *23*, 1273−1335.

(7) Stempfle, F.; Ortmann, P.; Mecking, S. Long-Chain Aliphatic Polymers To Bridge the Gap between Semicrystalline Polyolefins and Traditional Polycondensates. *Chem. Rev.* **2016**, *116*, 4597−4641.

(8) van der Meulen, I.; de Geus, M.; Antheunis, H.; Deumens, R.; Joosten, E. A. J.; Koning, C. E.; Heise, A. Polymers from Functional Macrolactones as Potential Biomaterials: Enzymatic Ring Opening Polymerization, Biodegradation, and Biocompatibility. *Biomacromolecules* **2008**, *9*, 3404−3410.

(9) Häußler, M.; Eck, M.; Rothauer, D.; Mecking, S. Closed-Loop Recycling of Polyethylene-like Materials. *Nature* **2021**, *590*, 423−427.

(10) de Ten Hove, C. L. F.; Penelle, J.; Ivanov, D. A.; Jonas, A. M. Encoding Crystal Microstructure and Chain Folding in the Chemical Structure of Synthetic Polymers. *Nat. Mater.* **2004**, *3*, 33−37.

(11) Menges, M. G.; Penelle, J.; de Ten Hove, C. L. F.; Jonas, A. M.; Schmidt-Rohr, K. Characterization of Long-Chain Aliphatic Polyesters: Crystalline and Supramolecular Structure of PE22,4 Elucidated by X-Ray Scattering and Nuclear Magnetic Resonance. *Macromolecules* **2007**, *40*, 8714−8725.

(12) Stempfle, F.; Ortmann, P.; Mecking, S. Which Polyesters Can Mimic Polyethylene? *Macromol. Rapid Commun.* **2013**, *34*, 47−50.

(13) Stempfle, F.; Ritter, B. S.; Mülhaupt, R.; Mecking, S. Long-Chain Aliphatic Polyesters from Plant Oils for Injection Molding, Film Extrusion and Electrospinning. *Green Chem.* **2014**, *16*, 2008.

(14) Marxsen, S. F.; Häußler, M.; Mecking, S.; Alamo, R. G. Isothermal Step Thickening in a Long-Spaced Aliphatic Polyester. *Polymer* **2020**, *191*, No. 122282.

(15) Kim, E.; Uyama, H.; Doi, Y.; Ha, C.-S.; Iwata, T. Crystal Structure and Morphology of Poly(11-Undecalactone) Solution-Grown Single Crystals. *Macromolecules* **2004**, *37*, 7258−7264.
(16) Kim, E.; Uyama, H.; Doi, Y.; Ha, C.-S.; Iwata, T. Crystal Structure and Morphology of Poly(12-Dodecalactone). *Biomacromolecules* **2005**, *6*, 572−579.
(17) Gazzano, M.; Malta, V.; Focarete, M. L.; Scandola, M.; Gross, R. A. Crystal Structure of Poly(ω-Pentadecalactone). *J. Polym. Sci., Part B: Polym. Phys.* **2003**, *41*, 1009−1013.
(18) Kim, E.; Uyama, H.; Doi, Y.; Ha, C.-S.; Iwata, T. Crystal Structure and Morphology of Poly(16-Hexadecalactone) Chain-Folded Lamellar Crystals. *Macromol. Biosci.* **2005**, *5*, 734−742.
(19) Armelin, E.; Almontassir, A.; Franco, L.; Puiggalí, J. Crystalline Structure of Poly(Decamethylene Sebacate). Repercussions on Lamellar Folding Surfaces. *Macromolecules* **2002**, *35*, 3630−3635.
(20) Vilela, C.; Silvestre, A. J. D.; Meier, M. A. R. Plant Oil-Based Long-Chain C 26 Monomers and Their Polymers. *Macromol. Chem. Phys.* **2012**, *213*, 2220−2227.
(21) Santonja-Blasco, L.; Zhang, X.; Alamo, R. G. Crystallization of Precision Ethylene Copolymers. *Adv. Polym. Sci.* **2017**, *276*, 133−182.
(22) Gaines, T. W.; Trigg, E. B.; Winey, K. I.; Wagener, K. B. High Melting Precision Sulfone Polyethylenes Synthesized by ADMET Chemistry. *Macromol. Chem. Phys.* **2016**, *217*, 2351−2359.
(23) Baughman, T. W.; Chan, C. D.; Winey, K. I.; Wagener, K. B. Synthesis and Morphology of Well-Defined Poly(Ethylene- Co -Acrylic Acid) Copolymers. *Macromolecules* **2007**, *40*, 6564−6571.
(24) Ortmann, P.; Lemke, T. A.; Mecking, S. Long-Spaced Polyamides: Elucidating the Gap between Polyethylene Crystallinity and Hydrogen Bonding. *Macromolecules* **2015**, *48*, 1463−1472.
(25) Kaner, P.; Ruiz-Orta, C.; Boz, E.; Wagener, K. B.; Tasaki, M.; Tashiro, K.; Alamo, R. G. Kinetic Control of Chlorine Packing in Crystals of a Precisely Substituted Polyethylene. Toward Advanced Polyolefin Materials. *Macromolecules* **2014**, *47*, 236−245.
(26) Zhang, X.; Santonja-Blasco, L.; Wagener, K. B.; Boz, E.; Tasaki, M.; Tashiro, K.; Alamo, R. G. Infrared Spectroscopy and X-Ray Diffraction Characterization of Dimorphic Crystalline Structures of Polyethylenes with Halogens Placed at Equal Distance along the Backbone. *J. Phys. Chem. B* **2017**, *121*, 10166−10179.
(27) Pepels, M. P. F.; Hansen, M. R.; Goossens, H.; Duchateau, R. From Polyethylene to Polyester: Influence of Ester Groups on the Physical Properties. *Macromolecules* **2013**, *46*, 7668−7677.
(28) Klonos, P. A.; Papadopoulos, L.; Kasimatis, M.; Iatrou, H.; Kyritsis, A.; Bikiaris, D. N. Synthesis, Crystallization, Structure Memory Effects, and Molecular Dynamics of Biobased and Renewable Poly(n -Alkylene Succinate)s with n from 2 to 10. *Macromolecules* **2021**, *54*, 1106−1119.
(29) Vonk, C. G.; Kortleve, G. X-Ray Small-Angle Scattering of Bulk Polyethylene. *Kolloid Z. Z. Polym.* **1967**, *220*, 19−24.
(30) Vonk, C. G.; Pijpers, A. P. An X-Ray Diffraction Study of Nonlinear Polyethylene. I. Room-Temperature Observations. *J. Polym. Sci., Polym. Phys. Ed.* **1985**, *23*, 2517−2537.
(31) Goderis, B.; Reynaers, H.; Koch, M. H. J.; Mathot, V. B. F. Use of SAXS and Linear Correlation Functions for the Determination of the Crystallinity and Morphology of Semi-Crystalline Polymers. Application to Linear Polyethylene. *J. Polym. Sci., Part B: Polym. Phys.* **1999**, *37*, 1715−1738.
(32) Roesle, P.; Stempfle, F.; Hess, S. K.; Zimmerer, J.; Río Bártulos, C.; Lepetit, B.; Eckert, A.; Kroth, P. G.; Mecking, S. Synthetic Polyester from Algae Oil. *Angew. Chem., Int. Ed.* **2014**, *53*, 6800−6804.
(33) Quinzler, D.; Mecking, S. Linear Semicrystalline Polyesters from Fatty Acids by Complete Feedstock Molecule Utilization. *Angew. Chem., Int. Ed.* **2010**, *49*, 4306−4308.
(34) Boz, E.; Wagener, K. B.; Ghosal, A.; Fu, R.; Alamo, R. G. Synthesis and Crystallization of Precision ADMET Polyolefins Containing Halogens. *Macromolecules* **2006**, *39*, 4437−4447.
(35) Smith, J. A.; Brzezinska, K. R.; Valenti, D. J.; Wagener, K. B. Precisely Controlled Methyl Branching in Polyethylene via Acyclic Diene Metathesis (ADMET) Polymerization. *Macromolecules* **2000**, *33*, 3781−3794.
(36) Matsui, K.; Seno, S.; Nozue, Y.; Shinohara, Y.; Amemiya, Y.; Berda, E. B.; Rojas, G.; Wagener, K. B. Influence of Branch Incorporation into the Lamella Crystal on the Crystallization Behavior of Polyethylene with Precisely Spaced Branches. *Macromolecules* **2013**, *46*, 4438−4446.
(37) Broadhurst, M. G. An Analysis of the Solid Phase Behavior of the Normal Paraffins. *J. Res. Natl. Bur. Stand., Sect. A: Phys. Chem.* **1962**, *66A*, No. 241.
(38) Yang, K.; Cai, Z.; Jaiswal, A.; Tyagi, M.; Moore, J. S.; Zhang, Y. Dynamic Odd-Even Effect in Liquid n -Alkanes near Their Melting Points. *Angew. Chem., Int. Ed.* **2016**, *55*, 14090−14095.
(39) Zhang, X.; Zuo, X.; Ortmann, P.; Mecking, S.; Alamo, R. G. Crystallization of Long-Spaced Precision Polyacetals I: Melting and Recrystallization of Rapidly Formed Crystallites. *Macromolecules* **2019**, *52*, 4934−4948.
(40) Zhang, X.; Marxsen, S. F.; Ortmann, P.; Mecking, S.; Alamo, R. G. Crystallization of Long-Spaced Precision Polyacetals II: Effect of Polymorphism on Isothermal Crystallization Kinetics. *Macromolecules* **2020**, *53*, 7899−7913.
(41) Pérez-Camargo, R. A.; Meabe, L.; Liu, G.; Sardon, H.; Zhao, Y.; Wang, D.; Müller, A. J. Even−Odd Effect in Aliphatic Polycarbonates with Different Chain Lengths: From Poly (Hexamethylene Carbonate) to Poly (Dodecamethylene Carbonate). *Macromolecules* **2021**, *54*, 259−271.
(42) Fritzsching, K. J.; Mao, K.; Schmidt-Rohr, K. Avoidance of Density Anomalies as a Structural Principle for Semicrystalline Polymers: The Importance of Chain Ends and Chain Tilt. *Macromolecules* **2017**, *50*, 1521−1540.
(43) Voigt-Martin, I. G.; Fischer, E. W.; Mandelkern, L. Morphology of Melt-Crystallized Linear Polyethylene Fractions and Its Dependence on Molecular Weight and Crystallization Temperature. *J. Polym. Sci., Polym. Phys. Ed.* **1980**, *18*, 2347−2367.
(44) Reimann, S.; Danke, V.; Beiner, M.; Binder, W. H. Synthesis of Supramolecular Precision Polymers: Crystallization under Conformational Constraints. *J. Polym. Sci., Part A: Polym. Chem.* **2017**, *55*, 3736−3748.
(45) Arrington, K. J.; Murray, C. B.; Smith, E. C.; Marand, H.; Matson, J. B. Precision Polyketones by Ring-Opening Metathesis Polymerization: Effects of Regular and Irregular Ketone Spacing. *Macromolecules* **2016**, *49*, 3655−3662.
(46) Tasaki, M.; Yamamoto, H.; Hanesaka, M.; Tashiro, K.; Boz, E.; Wagener, K. B.; Ruiz-Orta, C.; Alamo, R. G. Polymorphism and Phase Transitions of Precisely Halogen-Substituted Polyethylene. (1) Crystal Structures of Various Crystalline Modifications of Bromine-Substituted Polyethylene on Every 21st Backbone Carbon. *Macromolecules* **2014**, *47*, 4738−4749.
(47) Marxsen, S. F.; Häußler, M.; Mecking, S.; Alamo, R. G. Crystallization of Long-Spaced Precision Polyacetals III: Polymorphism and Crystallization Kinetics of Even Polyacetals Spaced by 6 to 26 Methylenes. *Polymers* **2021**, *13*, No. 1560.
(48) Zhao, J.; Wang, Z.; Niu, Y.; Hsiao, B. S.; Piccarolo, S. Phase Transitions in Prequenched Mesomorphic Isotactic Polypropylene during Heating and Annealing Processes As Revealed by Simultaneous Synchrotron SAXS and WAXD Technique. *J. Phys. Chem. B* **2012**, *116*, 147−153.
(49) Zhao, J.; Qiu, J.; Niu, Y.; Wang, Z. Evolutions of Morphology and Crystalline Ordering upon Annealing of Quenched Isotactic Polypropylene. *J. Polym. Sci., Part B: Polym. Phys.* **2009**, *47*, 1703−1712.
(50) Sorrentino, A.; Pantani, R.; Titomanlio, G. Crystallization of Syndiotactic Polystyrene under High Pressure and Cooling Rate. *Macromol. Res.* **2010**, *18*, 1045−1052.
(51) Rhoades, A. M.; Williams, J. L.; Androsch, R. Crystallization Kinetics of Polyamide 66 at Processing-Relevant Cooling Conditions and High Supercooling. *Thermochim. Acta* **2015**, *603*, 103−109.
(52) Cavallo, D.; Gardella, L.; Alfonso, G. C.; Portale, G.; Balzano, L.; Androsch, R. Effect of Cooling Rate on the Crystal/Mesophase

Polymorphism of Polyamide 6. *Colloid Polym. Sci.* **2011**, *289*, 1073−1079.
(53) Xie, Y.; Noda, I.; Akpalu, Y. A. Influence of Cooling Rate on the Thermal Behavior and Solid-State Morphologies of Polyhydroxyalkanoates. *J. Appl. Polym. Sci.* **2008**, *109*, 2259−2268.
(54) Snyder, R. G. Vibrational Spectra of Crystalline N-Paraffins. II. Intermolecular Effects. *J. Mol. Spectrosc.* **1961**, *7*, 116−144.
(55) Snyder, R. G.; Schachtschneider, J. H. Vibrational Analysis of the N-Paraffins—I. *Spectrochim. Acta* **1963**, *19*, 85−116.
(56) Snyder, R. G. Vibrational Spectra of Crystalline N-Paraffins. *J. Mol. Spectrosc.* **1960**, *4*, 411−434.
(57) Ortmann, P.; Mecking, S. Long-Spaced Aliphatic Polyesters. *Macromolecules* **2013**, *46*, 7213−7218.
(58) Pepels, M. P. F.; Govaert, L. E.; Duchateau, R. Influence of the Main-Chain Configuration on the Mechanical Properties of Linear Aliphatic Polyesters. *Macromolecules* **2015**, *48*, 5845−5854.
(59) Dannecker, P.-K.; Biermann, U.; Sink, A.; Bloesser, F. R.; Metzger, J. O.; Meier, M. A. R. Fatty Acid−Derived Aliphatic Long Chain Polyethers by a Combination of Catalytic Ester Reduction and ADMET or Thiol-Ene Polymerization. *Macromol. Chem. Phys.* **2018**, *220*, No. 1800440.
(60) Cao, Y.; Hu, G.; Lin, S.; Rempel, G. L.; Pan, Q. Synthesis of Precisely Diphenyl Ether-Functionalized Polyethylene via Acyclic Diene Metathesis Polymerization. *Polymer* **2019**, *175*, 41−48.
(61) Zhou, C.; Wei, Z.; Yu, Y.; Shao, S.; Leng, X.; Wang, Y.; Li, Y. Biobased Long-Chain Aliphatic Polyesters of 1,12-Dodecanedioic Acid with a Variety of Diols: Odd-Even Effect and Mechanical Properties. *Mater. Today Commun.* **2019**, *19*, 450−458.
(62) Jose, J.; Pourfallah, G.; Leao, A. L.; Narine, S. S. Influence of Monomeric and Polymeric Structure on the Physical Properties of Thermoplastic Polyesters Derived from Hydroxy Fatty Acids. *Polym. Int.* **2014**, *63*, 1902−1911.
(63) Cho, I.; Lee, K. Poly(Triacontamethylene Triacontanedioate) as Polyethylene Analogue: Properties and Enzymatic Degradation. *Macromol. Chem. Phys.* **1997**, *198*, 861−869.
(64) Ortmann, P. Nanocrystals and Models of Long-Spaced Polycondensates from Metathesis Polymerization of Functionalized Dienes. Doctoral Dissertation, Universität Konstanz: Konstanz, Germany, 2015.